Photoemission results on intralayer insertion at III-V/III-V junctions: A critical appraisal of the different interpretations

M. Moreno, M. Alonso, M. Höricke, R. Hey, K. Horn, J. L. Sacedón, K. H. Ploog, et al.

Citation: Journal of Vacuum Science & Technology B: Microelectronics and Nanometer Structures Processing, Measurement, and Phenomena **18**, 2128 (2000); doi: 10.1116/1.1306306

View online: https://doi.org/10.1116/1.1306306

View Table of Contents: https://avs.scitation.org/toc/jvn/18/4

Published by the American Institute of Physics

Photoemission results on intralayer insertion at III-V/III-V junctions: A critical appraisal of the different interpretations

M. Moreno[a)]
Instituto de Ciencia de Materiales de Madrid (CSIC), Cantoblanco, E-28049 Madrid, Spain, and Paul-Drude-Institut für Festkörperelektronik, Hausvogteiplatz 5-7, D-10117 Berlin, Germany

M. Alonso
Instituto de Ciencia de Materiales de Madrid (CSIC), Cantoblanco, E-28049 Madrid, Spain

M. Höricke and R. Hey
Paul-Drude-Institut für Festkörperelektronik, Hausvogteiplatz 5-7, D-10117 Berlin, Germany

K. Horn
Fritz-Haber-Institut der Max-Planck-Gesellschaft, D-14195 Berlin, Germany

J. L. Sacedón
Instituto de Ciencia de Materiales de Madrid (CSIC), Cantoblanco, E-28049 Madrid, Spain

K. H. Ploog
Paul-Drude-Institut für Festkörperelektronik, Hausvogteiplatz 5-7, D-10117 Berlin, Germany

(Received 17 January 2000; accepted 30 May 2000)

Several researchers have proposed that band discontinuities at semiconductor heterojunctions may be ''tuned'' by inserting very thin layers of foreign atoms at the interface which are thought to induce an ''interface dipole.'' Modifications of the *apparent* valence-band offset, as measured by photoelectron spectroscopy (PES), have been indeed observed upon Si insertion at GaAs–AlAs interfaces, and they have been generally interpreted as *real* band-offset changes. However, there is an alternative explanation of the photoemission results in terms of band-bending effects. Here, we present results of PES experiments designed to test the two opposing interpretations. We have examined the effect of Si insertion at polar (100) and nonpolar (110) interfaces, and we have studied the insertion of Si (*n*-type) and Be (*p*-type) intralayers. Similar results are obtained for polar and nonpolar interfaces, and effects of opposite sign are observed for Si and Be intralayers. These results can be readily interpreted in terms of a band-bending profile modification upon Si or Be insertion. Additional PES experiments performed at different substrate temperatures have allowed us to test the proposed band profiles. From the surface photovoltage effects induced at low temperature, we obtain evidence for sample band bending which is consistent with the room-temperature band profiles proposed. Hence, our results can be completely understood within a ''band-bending interpretation,'' calling into question the interpretation in terms of a ''band-offset tuning effect.''
© *2000 American Vacuum Society.* [S0734-211X(00)08104-X]

I. INTRODUCTION

Control of the magnitude of band offsets in semiconductor junctions may introduce a new degree of freedom in the design of heterojunction devices, and is thus a most desirable goal. Offsets of isovalent interfaces of type IV/IV, or III–V/III–V and II–VI/II–VI with a common anion or cation, have been found to be independent of orientation and interface quality.[1–5] At heterovalent junctions, such as III–V/IV junctions, band offsets seem to be determined by bulk properties for nonpolar interfaces, but they depend on interface microscopic details for polar orientations.[6] GaAs–AlAs interfaces, which have ubiquitous optoelectronic applications, belong to the group of common anion isovalent compound interfaces; therefore, the possibilities for changing the band offset in these interfaces are, in principle, limited. Nevertheless, it has been proposed[7,8] to modify the band discontinuity of these interfaces by inserting a group-IV (e.g., Si or Ge) intralayer, thus trying to convert the isovalent interface (III–V/III–V) into a double heterovalent one (III–V/IV+IV/III–V), so that a chance of modifying the band offset arises for polar interface orientations.

Two mechanisms have been proposed for the intralayer to induce a band-offset change. One is the establishment of charged interfaces of opposite polarity, the so called ''microscopic interface capacitor.'' Polar interfaces between heterovalent semiconductors, if ideally abrupt, should be charged. This situation is thermodynamically unstable but, if the intralayer is thin enough, the increase in the free energy of the system is small and the two heterovalent III–V/IV interfaces may remain charged,[9] and may act as the parallel plates of a microscopic capacitor [Fig. 1(a)].[10] The positively (negatively) charged interface corresponds to the side where the material is anion (cation) terminated. The establishment of this microscopic capacitor produces a potential drop at the interface, thus changing the band offset, ΔE_V, which increases or decreases depending on the stacking sequence [see

a)Electronic mail: mmoreno@icmm.csic.es

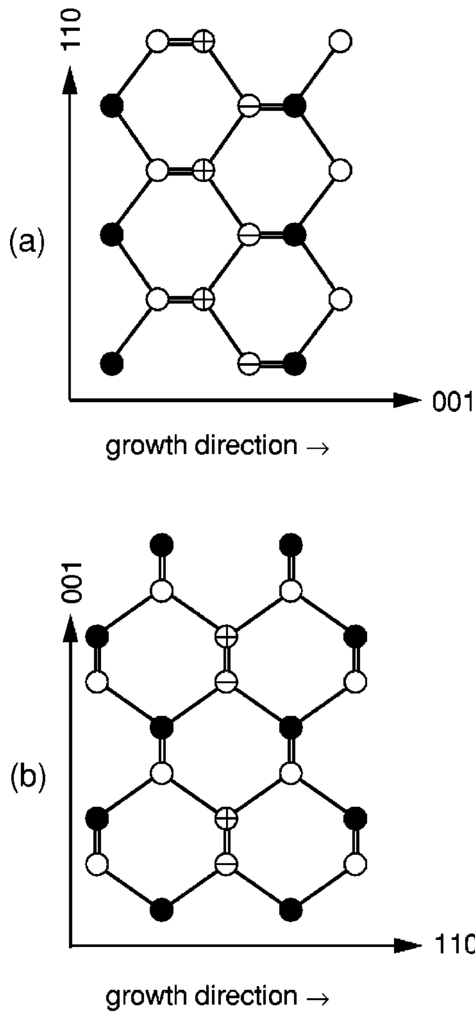

FIG. 1. Schematic representation of the charge transfer expected at (a) (100)-polar, and (b) (110)-nonpolar III–V/IV/III–V interfaces according to the Harrison microscopic interface-capacitor picture (Ref. 10).

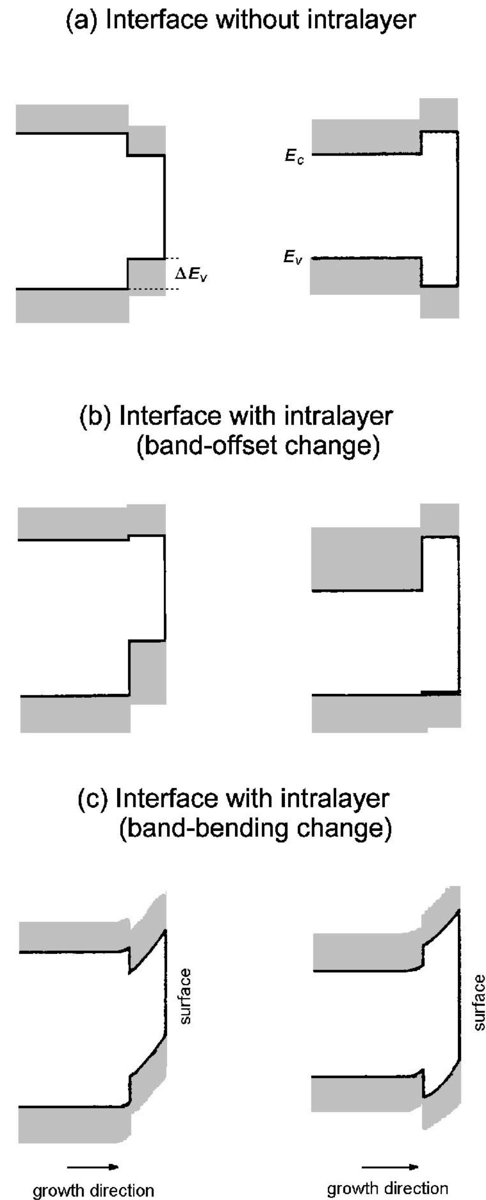

FIG. 2. Schematic band diagrams for GaAs-on-AlAs (left) and AlAs-on-GaAs (right) heterojunctions: (a) without an intralayer, and with a Si intralayer according to the two competing interpretations invoking (b) a band-offset charge or (c) a band-bending change.

Figs. 2(a) and 2(b)]. A second mechanism may lead to the formation of ''neutral nonequivalent interfaces.''[11] Reduction of the free energy of the system and neutrality are achieved through formation of point defects and atomic mixing.[10,12] Multiple interface configurations result from atomic mixing, thus producing different band-discontinuity values.[13,14] Within the microscopic-interface-capacitor picture,[10] the *polar* character of the interface plays a key role in the modification of the band offset. A polar geometry induces a charge transfer *crossing* the interface [Fig. 1(a)]. On the contrary, at nonpolar junctions the charge transfer takes place *along* but not *across* the interface [Fig. 1(b)]; thus, the layer-averaged interface is not charged. Hence, according to the microscopic-interface-capacitor model, band-offset changes are expected to occur upon intralayer insertion for polar interfaces but not for nonpolar ones.

Photoelectron spectroscopy (PES) is widely used to determine valence-band offsets at semiconductor heterointerfaces.[15–17] Determining the band discontinuity at the interface between two semiconductors, *A* and *B*, by core-level photoemission spectroscopy involves the measurement of the separation, $\Delta E_{\mathrm{CL}}=E_{\mathrm{CL}}^{B}-E_{\mathrm{CL}}^{A}$, between two core-level kinetic energies (relative to the Fermi level): E_{CL}^{A} and E_{CL}^{B}, corresponding to each side of the interface.[15–17] The valence-band offset ΔE_V^* is easily determined by subtracting a quantity, ξ, that accounts for the difference between the respective core-level binding energies:

$$\Delta E_V^* = \Delta E_{\mathrm{CL}} - \xi, \tag{1}$$

where

$$\xi = (E_{\mathrm{CL}}^{B} - E_V^{B}) - (E_{\mathrm{CL}}^{A} - E_V^{A}),$$

$E_{\mathrm{CL}} - E_V$ being the binding energy of the core level relative to the valence band maximum (VBM). The valence-band-

offset value, ΔE_V^*, determined in such a manner is called the ''apparent'' offset; it only corresponds to the *real* offset ΔE_V if certain conditions are met.

Determining interface band offsets requires one to prove *interface* energy values. However, photoemission spectroscopy provides weighted energy averages of emissions that originate all along the photoemission probing depth, not only at the interface. In order to guarantee that the energy values measured by photoemission correspond to those at the interface, flat-band conditions along the photoemission probing depth must prevail. The existence of band bending in this region gives rise to a systematic error in the determination of ΔE_V. Peak centroid positions can be used to define the kinetic energy values $E_{\rm CL}^A$ and $E_{\rm CL}^B$ included in Eq. (1). This choice fixes the accuracy in determining ΔE_V, because it does not discriminate the contribution from possible chemically shifted species, surface components, etc. Depending on the complexity of the core-level peaks and of the wanted accuracy, core-level peak deconvolution is or is not required.

Modifications of the *apparent* valence-band offset, as measured by PES, have been observed upon Si insertion at GaAs–AlAs interfaces,[18–22] and the microscopic-interface-capacitor model has sometimes been invoked to explain such changes.[18] However, since photoemission is sensitive to a variety of factors, it is important to establish whether a *real* band-offset change has occurred. In fact, an alternative interpretation of the PES results for the GaAs–(Si)–AlAs system has been proposed,[19,20] which assumes that the intralayer modifies the band-bending profile without changing the band offset. By relying solely on PES, it is difficult to assess whether the variations observed in the Al(2*p*)-to-Ga(3*d*) energy separation upon Si insertion at GaAs–AlAs(100) junctions[18–22] are due to modification of the interface band offset [Fig. 2(b)], or to variation of the band-bending profile near the surface [Fig. 2(c)]. Such band-bending effects are not easily measurable, or even detectable, by photoemission spectroscopy.[23,24] Nevertheless, one approach to investigating possible band-bending effects is to introduce intralayers of different doping type, since *n*-type and *p*-type impurities induce band bendings of opposite sign.

In order to accurately determine band discontinuities by photoemission spectroscopy, it is mandatory to perform the experiment under *flat-band* conditions, at least in the overlayer. Photovoltage effects have been shown to produce steady-state conditions in which the surface band bending is reduced or eliminated. Such surface photovoltage (SPV) effects can be induced by the light used to excite photoelectrons, e.g., by synchrotron light.[25–37] In this process, soft x-ray photons excite electrons to the conduction band, leaving holes in the valence band or core levels; secondary excitations and nonradiative decay processes effectively multiply the number of charge carriers. Electrons and holes are accelerated in opposite directions (photocurrent) by the built-in field present in the semiconductor depletion region, so that minority carriers accumulate at the surface. This carrier separation produces a photovoltage which opposes the initial built-in voltage. In order to maintain a charge balance, a current of majority carriers flows to the surface (restoring current). In equilibrium, the restoring current is equivalent and opposite to the photocurrent, so that both currents cancel each other. The supply of the restoring current is limited by the depletion region resistance, which has a pronounced dependence on sample temperature. At room temperature, the restoring current is usually sufficient to quickly discharge most of the induced photovoltage. However, at low temperature the restoring currents are reduced and there is a net forward bias. The surface photovoltage tends to eliminate any initial band bending present at the surface depletion region. Hence, comparison of synchrotron-radiation PES experiments performed at room and at low substrate temperatures may provide insight into the sample band bending.

Here, we follow a three-pronged approach in order to test the two opposing interpretations which have been proposed to explain the effect of intralayer insertion, i.e., intralayer-induced band-offset changes versus modifications of the band-bending profile [Figs. 2(b) and 2(c)]. According to the microscopic-interface-capacitor model,[10] qualitatively different behaviors are expected for polar and nonpolar interfaces. On the other hand, according to the band-bending interpretation, effects of opposite sign are expected for intralayers with *n*-type and *p*-type doping behaviors. In order to check whether the above predictions agree with experimental observations, we have first examined the effect of Si insertion at polar (100) and nonpolar (110) interfaces, and second we have studied the insertion of Si (*n*-type) and Be (*p*-type) intralayers. A third type of PES experiments, performed at low temperature, has permitted us to analyze the sample band profiles. While all three types of experimental results are seen to support a band-bending interpretation, some of them are in conflict with an interpretation invoking band-offset changes.

II. EXPERIMENT

Using molecular-beam epitaxy (MBE), we have fabricated GaAs/AlAs heterojunctions on (100)-[2° off toward (111) *A*] and (110) GaAs substrates. We used epiready heavily Si-doped ($n = 1\times10^{18}$ cm^{-3}) substrates to prevent the samples from being charged during the photoemission measurements. First, a (0.1–0.3)-μm-thick Si-doped GaAs buffer layer was grown ($n = 1\times10^{18}$ cm^{-3}), followed by a 20-nm-thick undoped AlAs layer [Fig. 3(a)]. At this point, a layer of Si or Be, with a density of 2.2×10^{14} atoms cm^{-2}, was inserted in some of the samples. This two-dimensional (2D) concentration corresponds to approximately 1/3 of the atomic sites in a (100) monolayer, or to 1/4 of the atomic sites in a (110) monolayer. Finally, all samples were terminated by a 2-nm-thick, nominally undoped, GaAs overlayer [Fig. 3(a)]. The growth parameters employed are summarized in Tables I and II. The conditions for growth on (110) substrates were carefully optimized by using atomic-force microscopy to guarantee a smooth surface morphology. The Si and Be intralayers were inserted using a *pulsed low-flux* δ-doping method.[38,39] In the samples containing an intralayer

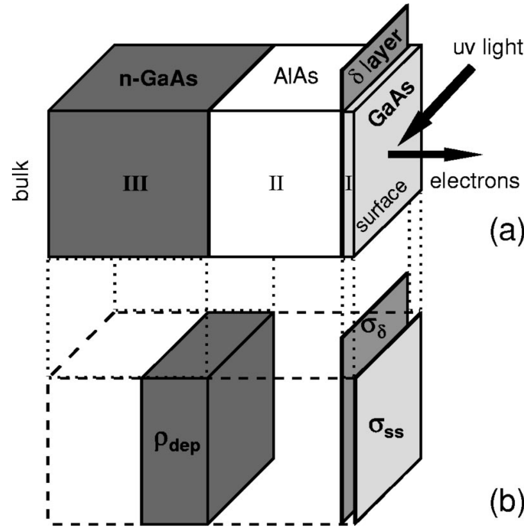

FIG. 3. (a) Schematic representation of the sample structure. (b) Model charge configuration assumed in the calculations.

of Si or Be, the overlayer was grown at a reduced substrate temperature to minimize segregation and outdiffusion of intralayer atoms.

After growth, the samples were transferred under ultra high vacuum from the MBE chamber to the PES station at the synchrotron source using a small transfer chamber. The samples were placed together in the analysis chamber, under electrical contact and grounded. We used a multiple sample holder which accommodated several samples. One of the holder positions was designed to be in thermal contact with a liquid-N_2 reservoir. The low-temperature (LT) measurements were carried out by placing the sample to be analyzed in this cooling position. The temperature at which the samples were cooled down in this way corresponds to a thermocouple reading of 220 K. Equal LT conditions were reproducibly obtained with this cooling arrangement, the actual temperature being probably lower than the nominal.

PES measurements were performed immediately after sample growth using synchrotron radiation coming from the TGM2 and TGM6 beamlines of BESSY I (Berliner Elektronenspeicherring-Gesellschaft für Synchrotronstrahlung mbH). The low-temperature experiments were performed using radiation from the TGM6 monochromator, which was located in front of a wiggler/undulator, delivering $10^{12}-10^{13}$ photons/s in the photon energy range used (40–95 eV). Electron kinetic-energy distribution curves (EDCs) were obtained for each sample. The Ga(3*d*), Al(2*p*), As(3*d*) and valence-band-edge emissions from each sample, as well as the Fermi-edge emission from a gold foil that was in electrical contact with the back side of the semiconductor samples, were consecutively recorded at a fixed photon energy. This procedure was repeated for several photon energies. Electrons were collected and counted in normal-emission geometry by an angle-resolving photoelectron spectrometer. The overall energy resolution was 150–300 meV over the range of photon energies used.

III. RESULTS AND DISCUSSION

A. Polar versus nonpolar interface orientations

Figure 4 shows Al(2*p*) and Ga(3*d*) EDC spectra recorded from GaAs-on-AlAs heterostructures with 95 eV photons. Results from samples without (closed symbols) and with (open symbols) a Si intralayer are compared for the (100) [Fig. 4(a)] and (110) [Fig. 4(b)] interface orientations. The Fermi-edge spectrum recorded on gold is also displayed. Upon Si insertion, the Ga(3*d*) peak from the GaAs overlayer

TABLE I. MBE-growth parameters of the samples studied in Sec. III A.

	GaAs/AlAs(100)	GaAs/Si/AlAs(100)	GaAs/AlAs(110)	GaAs/Si/AlAs(110)
Substrate (GaAs)				
orientation	(100)-2°→(111)*A*	(100)-2°→(111)*A*	(110)	(110)
Si doping	1×10^{18} cm^{-3}	1×10^{18} cm^{-3}	1×10^{18} cm^{-3}	1×10^{18} cm^{-3}
Buffer layer (GaAs)				
thickness	0.3 μm	0.3 μm	0.1 μm	0.1 μm
T_{subs}	590 °C	590 °C	485 °C	485 °C
growth rate	0.44 μm/h	0.44 μm/h	0.16 μm/h	0.16 μm/h
Si doping	1×10^{18} cm^{-3}	1×10^{18} cm^{-3}	1×10^{18} cm^{-3}	1×10^{18} cm^{-3}
Buried layer (AlAs)				
thickness	20.0 nm	20.0 nm	20.0 nm	20.0 nm
T_{subs}	610 °C	610 °C	505 °C	505 °C
growth rate	0.36 μm/h	0.36 μm/h	0.18 μm/h	0.18 μm/h
Si doping	⋯	⋯	⋯	⋯
Intralayer		(Si)		(Si)
2D density	⋯	2.2×10^{14} cm^{-2}	⋯	2.2×10^{14} cm^{-2}
T_{subs}	⋯	590 °C	⋯	505 °C
flux (pulsed)	⋯	2×10^{11} cm^{-2} s^{-1}	⋯	2×10^{11} cm^{-2} s^{-1}
Overlayer (GaAs)				
thickness	2.0 nm	2.0 nm	2.0 nm	2.0 nm
T_{subs}	590 °C	540 °C	505 °C	385-485 °C
growth rate	0.44 μm/h	0.44 μm/h	0.16 μm/h	0.16 μm/h
Si doping	⋯	⋯	⋯	⋯

TABLE II. MBE-growth parameters of the samples studied in Secs. III B and III C.

	GaAs/AlAs(100)	GaAs/Si/AlAs(100)	GaAs/Be/AlAs(100)
Substrate (GaAs)			
orientation	(100)-2°→(111)*A*	(100)-2°→(111)*A*	(100)-2°→(111)*A*
Si doping	1×10^{18} cm^{-3}	1×10^{18} cm^{-3}	1×10^{18} cm^{-3}
Buffer layer (GaAs)			
thickness	0.3 μm	0.3 μm	0.3 μm
T_{subs}	590 °C	590 °C	590 °C
growth rate	0.2 μm/h	0.2 μm/h	0.2 μm/h
Si doping	1×10^{18} cm^{-3}	1×10^{18} cm^{-3}	1×10^{18} cm^{-3}
Buried layer (AlAs)			
thickness	20.0 nm	20.0 nm	20.0 nm
T_{subs}	610 °C	610 °C	610 °C
growth rate	0.2 μm/h	0.2 μm/h	0.2 μm/h
Si doping	⋯	⋯	⋯
Intralayer		(Si)	(Be)
2D density	⋯	2.2×10^{14} cm^{-2}	2.2×10^{14} cm^{-2}
T_{subs}	⋯	590 °C	500 °C
flux (pulsed)	⋯	2×10^{11} cm^{-2} s^{-1}	2×10^{11} cm^{-2} s^{-1}
Overlayer (GaAs)			
thickness	2.0 nm	2.0 nm	2.0 nm
T_{subs}	610 °C	540 °C	450 °C
growth rate	0.2 μm/h	0.2 μm/h	0.2 μm/h
Si doping	⋯	⋯	⋯

remains at nearly the same position, while the Al($2p$) peak from the AlAs buried layer shifts towards lower kinetic energies. Thus, the Al($2p$)-to-Ga($3d$) energy distance increases upon Si insertion. Remarkably, this effect is observed for *both* polar-(100) and nonpolar-(110) interfaces.

We have determined the apparent valence-band offset, ΔE_V^*, from the core-level offset, ΔE_{CL}, measured between the Al($2p$) and Ga($3d$) peak centroids, the ''centroid'' being defined as the energy value that divides the peak into two parts of equal area. We have used in Eq. (1) a value for ξ of 54.00 eV, calculated considering the well known Ga($3d$) binding energy in GaAs (−18.86 eV) and Al($2p$) binding energy in AlAs (−72.86 eV). The contribution of chemically shifted species and surface/interface components is expected to be small in our GaAs/AlAs heterostructures. For the heterojunctions without an intralayer, the apparent valence-band offsets are 0.50 eV and 0.48 eV for the (100) and (110) orientations, respectively. The apparent valence-band offset obtained for (100) Si-containing heterostructures is 1.12 eV, that is, for the (100) orientation ΔE_V^* increases by 0.62 eV upon Si insertion. For (110) Si-containing heterostructures the apparent valence-band offset is 0.81 eV, that is, for the (110) orientation ΔE_V^* increases by 0.33 eV upon Si insertion.

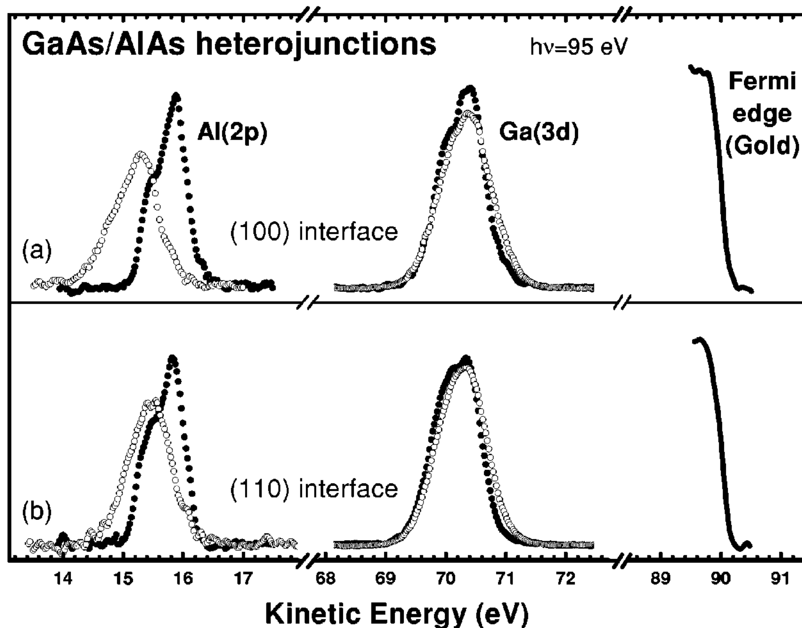

FIG. 4. Al($2p$) and Ga($3d$) core-level spectra recorded on GaAs/AlAs (closed circles) and GaAs/Si/AlAs (open circles) heterojunctions (GaAs on top), with 95 eV photons. Results for (a) (100), and (b) (110)-oriented interfaces. Fermi-edge spectra recorded on gold are also shown. The core-level spectra are normalized to the peak area.

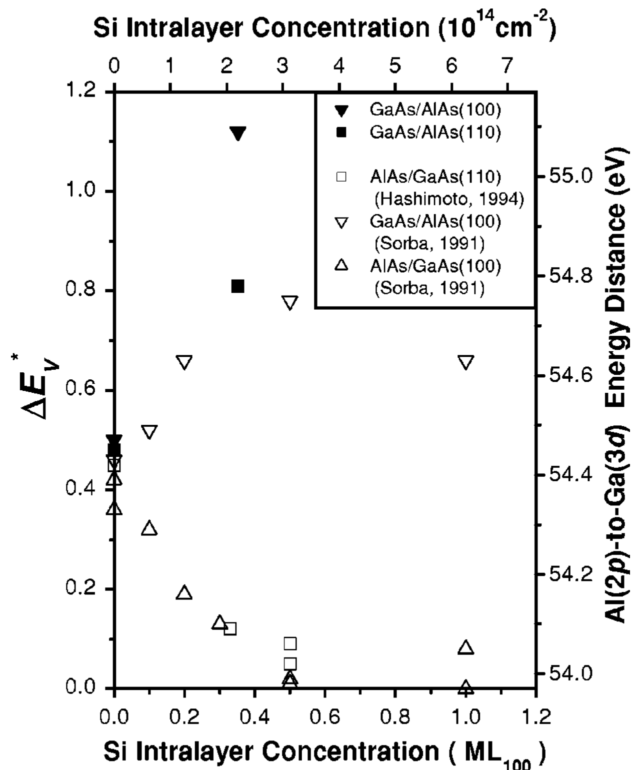

FIG. 5. *Apparent* valence-band offset and corresponding Al(2p)-to-Ga(3d) separation measured by photoemission spectroscopy on AlAs–Si–GaAs heterostructures. Our results (closed symbols) and those reported by other groups (open symbols) are shown as a function of the nominal Si-intralayer concentration for different interface orientations and stacking sequences.

Figure 5 shows a comparison of our results (closed symbols) with results obtained by other groups for the AlAs–GaAs system (open symbols). The apparent valence-band offset that we have obtained for Si-containing (100) interfaces (1.12 eV) is markedly higher than the value previously reported for the same nominal Si concentration [0.65 eV for 1/3 monolayer (ML)],[18] which we attribute to our improved method of Si deposition. Our results for GaAs-on-AlAs(110) junctions, together with the data reported[2] for the reverse stacking sequence, AlAs-on-GaAs(110), indicate that the apparent valence-band offset in nonpolar interfaces *increases* or *decreases* depending on the stacking sequence, similar to what was previously found for polar interfaces.[18]

Geometric arguments, such as those included in the microscopic-interface-capacitor model, do not explain why the band offset should change at nonpolar interfaces. The chemical asymmetry existing between each side of the interface (AlAs versus GaAs) could account for a Si-induced dipole *crossing* a nonpolar interface. However, if this explanation were valid, the same increase or decrease of the band offset should occur at the nonpolar interface independently of the stacking sequence. Muñoz and Rodríguez-Hernández predicted[40] a *reduction* of the valence-band offset at AlAs–GaAs (110) interfaces upon Si insertion. According to their calculations, the same reduction of the offset should occur for GaAs-on-AlAs and AlAs-on-GaAs junctions because, since this type of calculation does not take into account the presence of the surface, both stacking sequences are indistinguishable in the case of the (110) orientation. Thus, the *increase* or *decrease* of the apparent band offset depending on the stacking sequence observed for (110) nonpolar interfaces is explained neither by the microscopic-interface-capacitor model, nor by the chemical asymmetry of the junction, nor by the calculations of Muñoz and Rodríguez-Hernández. A model based on the establishment of ''neutral nonequivalent interfaces,'' like that recently proposed by Miwa and Ferraz,[41] could probably account for band-offset changes occurring at nonpolar interfaces. Actually, whatever the experimental result was, one could likely find a suitable ''disordered interface atomic configuration'' giving rise to a theoretical offset in agreement with experiment.[11] Arguments invoking ''neutral nonequivalent interfaces'' as responsible of band-offset changes must prove, in order to be solid, that the selected interface atomic configuration corresponds to the configuration of the real samples.

The results summarized in Fig. 5 can be readily understood within a band-bending interpretation,[19,20,22] without requiring a band-offset change altogether, as follows. The n-type doping character of the Si intralayer induces a sharp upward band bending in the overlayer [Fig. 2(c)]. This bending is reflected in an increase (decrease) of the Al(2p)-to-Ga(3d) energy distance measured by PES for GaAs-on-AlAs (AlAs-on-GaAs) heterostructures, as further explained below, the polarity nature of the interface being irrelevant.

B. n-type versus p-type intralayers

Figure 6 shows Al(2p), Ga(3d) and valence-band-edge spectra recorded with 95 eV photons on different GaAs-on-AlAs(100) heterostructures: (i) without intralayer (closed symbols), (ii) with a Si intralayer [open symbols in Fig. 6(a)], and (iii) with a Be intralayer [open symbols in Fig. 6(b)]. The Al(2p)-to-Ga(3d) energy separation is observed to *increase* upon Si insertion and to *decrease* upon Be insertion. The apparent valence-band offset ΔE_V^* increases by 0.59 eV upon Si insertion, and decreases by 0.19 eV upon Be insertion. The gold spectrum permits us to determine the location of the Fermi level deep in the bulk of the semiconductor samples; for equilibrium room-temperature measurements it also defines the location of the Fermi level at the sample surface. This is very useful information because it can be used as an absolute reference for the measurements performed in the different samples. The surface Fermi level is observed to lie 0.95 eV above the VBM in GaAs/AlAs(100) heterostructures without an intralayer, 0.78 eV in GaAs/Si/AlAs(100), and 1.09 eV in GaAs/Be/AlAs(100) (Fig. 6); the surface Fermi level thus approaches the VBM by 0.17 eV upon Si insertion, and shifts away by 0.14 eV upon Be insertion. Hence, the experimental results reveal an opposite behavior of the core-level separation and of the surface Fermi-level position for Si and Be insertions, which is qualitatively consistent with an interpretation in terms of band-bending effects and a doping role for the inserted impurities. They are also quantitatively consistent, as we show below.

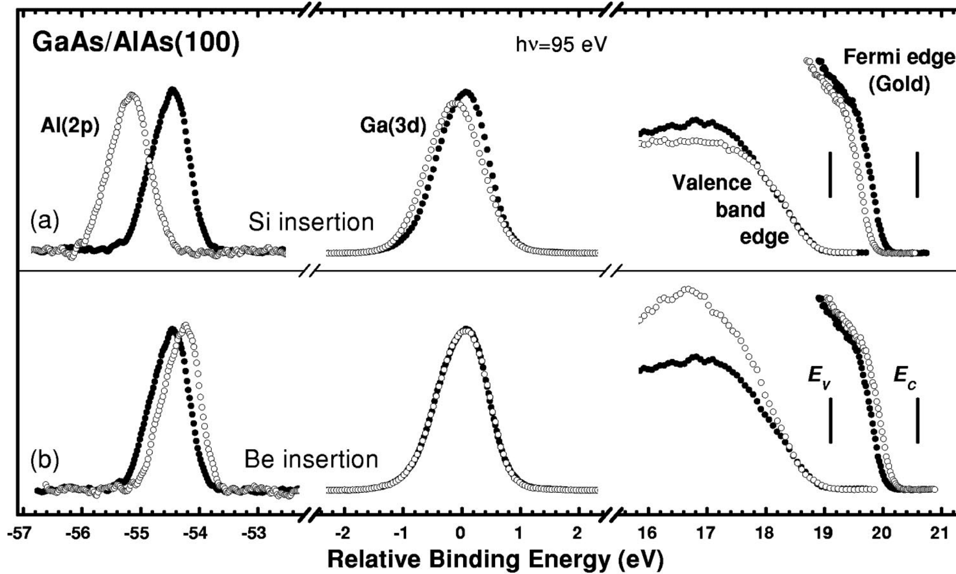

FIG. 6. Al(2*p*), Ga(3*d*) and valence-band-edge EDC spectra recorded with 95 eV photons on GaAs-on-AlAs(100) heterojunctions without (closed circles) and with (open circles) an intralayer, as well as Fermi-edge spectrum recorded on gold. The effects of (a) Si and (b) Be insertions are compared. Data are presented in a relative binding-energy scale, where the leading edges of the valence-band spectra recorded in the different samples have been aligned, and the energy zero has been arbitrarily chosen at the position of the Ga(3*d*) centroid of the sample without an intralayer. The core-level spectra are normalized to the peak area.

Our samples include three well-distinguished regions: (i) the GaAs *n*-doped substrate (region III), (ii) the AlAs buried layer (region II), and (iii) the GaAs overlayer (region I) [see Fig. 3(a)]. Some samples contain a Si or a Be δ layer at the front GaAs/AlAs interface, between layers I and II. We have calculated the band profiles along the different regions by solving Poisson's equation for *model* charge distributions appropriate to each type of sample, and introducing as input parameters the positions of the Fermi level deep in the bulk of the sample and at the surface. Deep in the bulk, the Fermi level lies close to the conduction-band minimum (CBM) due to the high *n*-type doping of the substrates. For the surface Fermi-level positions we have considered those experimentally determined for each type of sample.

In heterostructures without an intralayer we have assumed the following charge distribution: (i) a laminar charge located at the surface due to the charge trapped in surface states (σ_{SS}) and (ii) a volume charge located at the shallowest part of the Si-doped GaAs substrate, which consists of a homogeneous distribution of positively ionized Si atoms (ρ_{dep}); see Fig. 3(b). The corresponding band profile is displayed in Fig. 7(a). For heterostructures without an intralayer band bending takes place mainly along the AlAs buried layer, and the potential varies very little along the GaAs overlayer, only 0.03 V.

Accounting for the doping role of Si and Be impurities in GaAs, we have assumed that in our intralayer-containing samples a certain fraction of the inserted Si (Be) atoms becomes positively (negatively) ionized, with electrons (holes) being released to the host semiconductor lattice. Such a fraction of ionized intralayer atoms will be called the ''effective doping concentration.'' Although the exact distribution of the intralayer atoms is unknown and some segregation and outdiffusion are expected to occur, a certain fraction of the inserted atoms likely remains localized at the interface position. For simplification, we have assumed that all the intralayer atoms acting as dopants (effective doping concentration) are confined at the interface position. Although this assumption is not expected to exactly match the real situation, since some of the outdiffused atoms could also have a doping role, it serves us to illustrate the physics of the process.

In our samples, the δ layer has been inserted at the front GaAs/AlAs interface (I/II interface), which is located only 2 nm from the surface. According to the hydrogen model, the first-orbit radius of impurity electrons (holes) in GaAs amounts to 10 nm (3 nm). Due to the close proximity of the surface, most of the impurity electrons (holes) provided by the Si (Be) intralayer are probably trapped in surface states.[42] Therefore, in our intralayer-containing heterostructures we have considered, besides a substrate volume charge ρ_{dep}, a static *capacitor-like* charge distribution [schematically depicted in Fig. 3(b)], where the electrons (holes) provided by the intralayer are trapped in surface states, thus *separated* from their parent Si (Be) atoms; a positively (negatively) charged sheet σ_{δ}, located at the interface position, represents the charge of the ionized Si (Be) atoms, and a sheet σ_{SS} represents the surface charge.

The band bending across the overlayer region can be calculated for a specific intralayer charge density or, conversely, one can calculate the intralayer charge density that produces a certain potential variation across the overlayer. We have calculated the number of ionized intralayer atoms required to induce a variation in the magnitude of the overlayer band bending that equals the changes observed in the Al(2*p*)-to-Ga(3*d*) offset displayed in Fig. 6. According to our calculations, a concentration of 2.39×10^{13} atoms cm^{-2} (7.4×10^{12} atoms cm^{-2}) must be positively (negatively) ionized to account for the experimental results obtained for insertion of Si (Be) at (100) interfaces. Figures 7(b) and 7(c) display the band profiles calculated for heterostructures with the above intralayer charge densities. It can be seen that the *n*-type Si δ layer induces sharp *upward* overlayer band bending, while

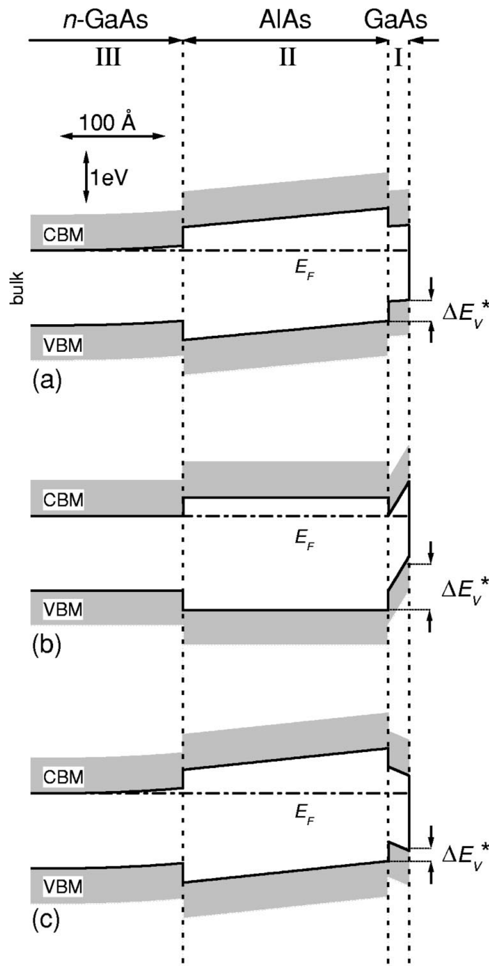

FIG. 7. Band profiles in our (a) GaAs/AlAs(100), (b) GaAs/Si/AlAs(100), and (c) GaAs/Be/AlAs(100) heterostructures. They have been calculated considering the model charge distribution shown in Fig. 3(b). An effective doping concentration of 2.39×10^{13} cm^{-2} has been assumed for the case of Si, and of 7.4×10^{12} cm^{-2} for the case of Be. The *apparent* valence-band offsets, ΔE_V^*, that would be measured by photoemission for the band profiles displayed are also shown. The horizontal lines at the right indicate the valence-band-maximum positions obtained by subtracting from the $\overline{E_{\mathrm{Al}(2p)}}$ and $\overline{E_{\mathrm{Ga}(3d)}}$ PES average energies the respective core-level binding energies.

the *p*-type Be δ layer causes *downward* overlayer band bending.

In order to understand how such intralayer-induced modifications of the band profile alter the Al($2p$)-to-Ga($3d$) energy separation measured in a photoemission experiment, it is important to realize that the PES signal is the result of adding up emissions from atoms located at different depths, each contribution being weighted by an exponential factor, which accounts for the attenuation of the signal due to the electron scattering. The PES average energy of a core level $\overline{E_{\mathrm{CL}}}$ can be written as follows:

$$\overline{E_{\mathrm{CL}}}=\frac{\int_0^\infty E_{\mathrm{CL}}(z)\exp(-z/\lambda)\mathrm{d}z}{\int_0^\infty \exp(-z/\lambda)\mathrm{d}z}, \tag{2}$$

where E_{CL} (z) is the energy of the core level as a function of the depth z, and λ is the photoelectron attenuation length. Hence, PES probes a certain volume of the sample close to the surface, strongly enhancing the signals coming from shallow regions over those originating in the deep layers. The PES average energy of the Ga($3d$) core level, $\overline{E_{\mathrm{Ga}(3d)}}$, essentially corresponds to the value of $E_{\mathrm{Ga}(3d)}$ at the surface, being not very sensitive to energy variations along the GaAs overlayer. $\overline{E_{\mathrm{Ga}(3d)}}$ mainly reflects the variations in the Fermi-level surface pinning position. The PES average energy of the Al($2p$) core level, $\overline{E_{\mathrm{Al}(2p)}}$, corresponds to the value of $E_{\mathrm{Al}(2p)}$ at the shallowest part of the AlAs region, being not very sensitive to energy variations along the AlAs buried layer. $\overline{E_{\mathrm{Al}(2p)}}$ is much more sensitive to changes of the overlayer band bending than $\overline{E_{\mathrm{Ga}(3d)}}$; in fact, $\overline{E_{\mathrm{Al}(2p)}}$ is shifted by the same energy amount as the magnitude of the potential drop in the overlayer. Figure 7 shows the *apparent* valence-band offsets, ΔE_V^*, that would be measured by photoemission for samples with the band profiles displayed. The horizontal lines at the right of Fig. 7 indicate the valence-band-maximum positions obtained by subtracting from $\overline{E_{\mathrm{Al}(2p)}}$ and $\overline{E_{\mathrm{Ga}(3d)}}$ the respective core-level binding energies. Note that ΔE_V^* does not correspond to the real interface valence-band offset; ΔE_V^* is strongly affected by the overlayer band bending, an upward (downward) bending of the overlayer bands resulting in a larger (shorter) value of ΔE_V^*.

From the above model calculations we infer that about 2×10^{13} Si atoms cm^{-2} (7×10^{12} Be atoms cm^{-2}) must be ionized in the Si (Be) intralayer to account for the observed Al($2p$)-to-Ga($3d$) offset variations on the basis of a band-bending effect. Such *effective doping* concentration has a direct relation to the *free-carrier* concentration determined by Hall-effect measurements. Hall-effect experiments indicated that the *pulsed low-flux* impurity-deposition recipe that we have used permits one to obtain carrier concentrations in the 10^{13} cm^{-2} range for Si δ-layer atomic concentrations in the high-10^{13}/low-10^{14}) atoms cm^{-2} range.[38,39] Thus, the effective doping concentrations necessary to explain the experimental results on the basis of a band-bending effect are actually achieved.

It is thus possible to successfully explain the observed *apparent* valence-band offset variations (Fig. 6) solely on the basis of intralayer-induced modifications of the overlayer band bending, with no need to include any change of the *real* interface band offset. In our interpretation the overlayer band bending results from trapping of the carriers provided by the intralayer in surface states, being thus separated from their ionized parent intralayer atoms. Segregation of intralayer atoms and *bulk* doping are not necessary for the build up of an overlayer band bending, just a separation of charges across the overlayer (overlayer capacitor effect) is needed. The band-bending interpretation provides a straightforward explanation for the fact that Si and Be intralayers induce changes of opposite sign: this can be easily understood accounting for the respective *n*-type and *p*-type doping behaviors.

The overlayer-capacitor model that we have used to illustrate the band-bending interpretation differs substantially from the interface-capacitor model previously invoked to explain the proposed intralayer-induced band-offset changes.

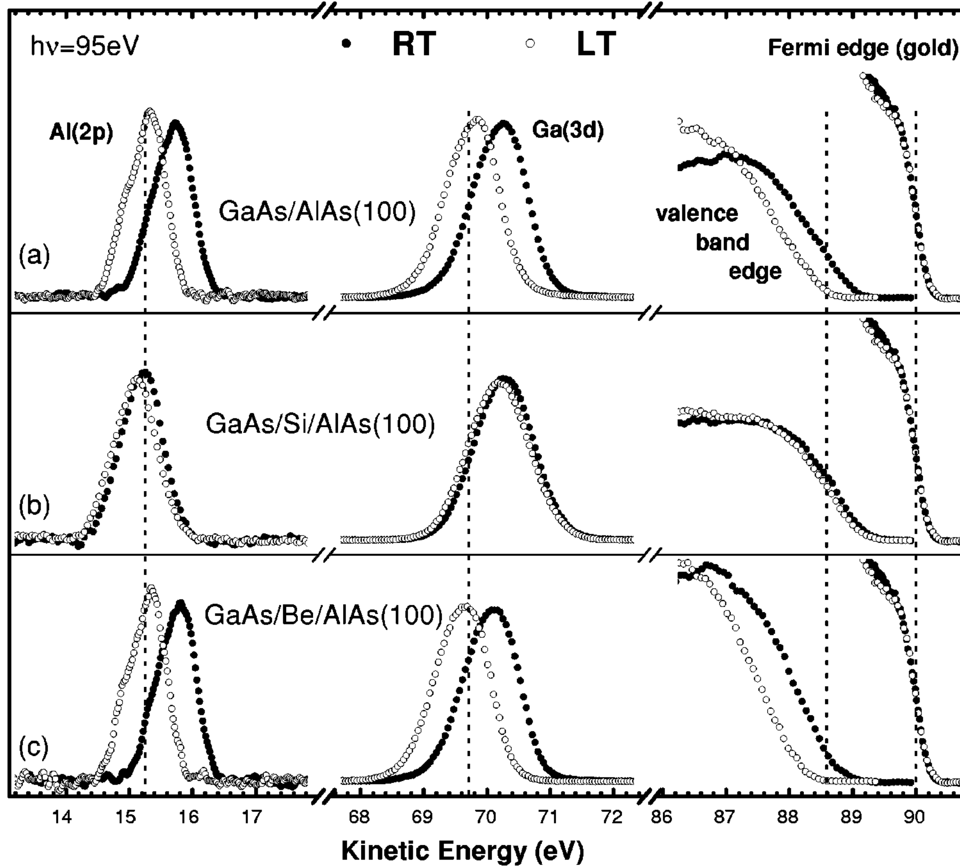

FIG. 8. Al(2p), Ga(3d) and valence-band-edge EDC spectra recorded with 95 eV photons at room temperature (closed circles) and at low temperature $T \sim 220$ K (open circles) on (a) GaAs/AlAs(100), (b) GaAs/Si/AlAs(100), and (c) GaAs/Be/AlAs(100) heterostructures. Gold Fermi-edge spectra are also shown. The core-level spectra are normalized to the peak area. The vertical dotted lines mark the kinetic-energy positions corresponding to the Al(2p), Ga(3d), and valence-band-maximum levels under flat-band conditions, as well to the *bulk* Fermi level.

The polarity nature of the interface plays a key role within the interface-capacitor model, but it is not important for the model here proposed, as long as the properties of the growth on different substrate orientations do not change the effective doping concentration. We have observed Si-induced core-level offset variations that are larger for polar GaAs/AlAs(100) junctions than for nonpolar GaAs/AlAs(110) ones (Fig. 4). This result can be well understood within the band-bending interpretation, since the strength of the overlayer-capacitor effect depends on the *effective doping* concentration of the intralayer; such a concentration is expected to be higher in (100)-oriented samples than in (110)-oriented ones, for two reasons: (i) because self-compensation is known to be more important for growth on (110) substrates[43] and (ii) because the Si-insertion recipe used here was specifically optimized for the (100) growth direction.[38] Figure 5 shows that the core-level offset variation that we have observed upon Si insertion at GaAs-on-AlAs(100) junctions is remarkably larger than the changes previously reported by other groups. Such an observation can be also explained within the band-bending interpretation: the larger effect is likely due to the higher doping efficiency of our pulsed low-flux Si-deposition technique in comparison with the growth recipes employed by other groups.

Although the position of the intralayer with respect to the surface is irrelevant within the interface-capacitor model, it plays a key role in our overlayer-capacitor model. No differences in the strength of the microscopic interface capacitor are in principle expected between the samples used in PES experiments and in devices. However, charge separation in the overlayer and the associated band bending occurs only if a certain number of the carriers provided by the intralayer becomes trapped in surface states, which requires that the intralayer is located close enough to the surface. Although such a condition is easily fulfilled in samples typically analyzed in a photoemission experiment, the relevance of the overlayer-capacitor effect is not clear for the type of heterojunctions with deeply buried interfaces that are generally used in devices.

C. Surface photovoltage effects

Surface photovoltage effects can have a strong influence on the kinetic energies measured by photoemission for core levels of semiconductor materials.[25,29,34] Figures 8(a)–8(c) show Al(2p), Ga(3d), and valence-band-edge spectra recorded with 95 eV photons at room and at low temperature (RT and LT) on GaAs-on-AlAs(100) heterostructures without an intralayer, with a Si intralayer, and with a Be intralayer, respectively. Figure 8 also shows gold Fermi-edge spectra. The LT signals from the GaAs/AlAs(100) and GaAs/Be/AlAs(100) heterostructures appear significantly shifted relative to the RT emissions. In contrast, for the GaAs/Si/AlAs(100) heterostructure the PES signals scarcely shift upon cooling (<0.1 eV). The Al(2p), Ga(3d), and valence-band-edge signals *rigidly* shift by 0.43 and 0.47 eV toward lower kinetic energies for the GaAs/AlAs(100) and

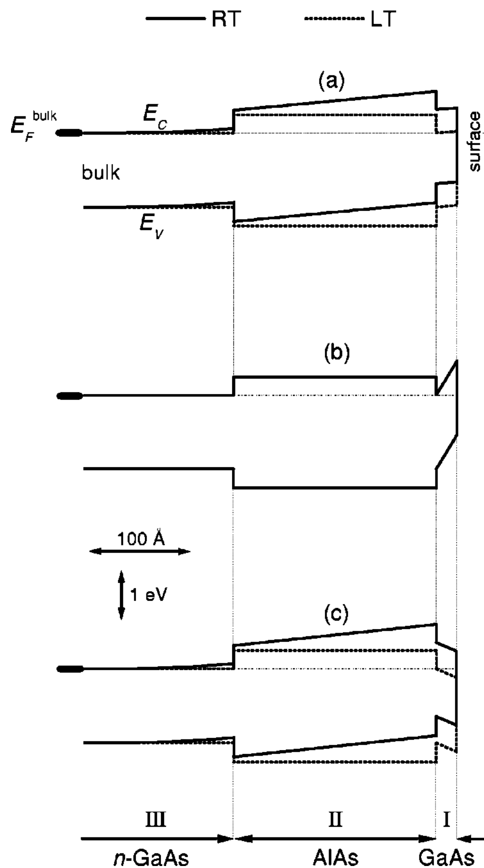

FIG. 9. Band profiles proposed for (a) GaAs/AlAs(100), (b) GaAs/Si/AlAs(100), and (c) GaAs/Be/AlAs(100) heterostructures, when illuminated with 95 eV photons at room temperature (solid lines) and low temperature (dotted lines). The horizontal dash-dotted thin lines mark the energy position of the Fermi level *deep in the bulk* of the samples.

GaAs/Be/AlAs(100) heterostructures, respectively. Noticeably, for the three types of samples, the Al(2*p*)-to-Ga(3*d*) energy separations measured at LT are *identical* to those measured at RT, and the Al(2*p*) peaks approximately converge upon cooling on a common energy position.

The shifts of the PES signals observed upon cooling (Fig. 8) can be explained by the occurrence of photoinduced nonequilibrium processes at LT, which modify the RT band profiles. Since light penetrates even into the *n*-GaAs substrate, SPV effects can in principle occur in the GaAs overlayer, the AlAs buried layer, and even in a portion of the *n*-GaAs substrate. The temperature-dependent results can be understood by considering light-induced modifications of the proposed RT band profiles (Fig. 7), so that at LT bands become completely flat in the AlAs region, and the band bending in the GaAs overlayer persists (see the LT profiles displayed in Fig. 9 as dotted lines).

According to the band profile proposed for the GaAs/Si/AlAs(100) heterostructure at RT [solid lines in Fig. 9(b)], the bands are flat along the AlAs region. There is thus no reason for induction of a photovoltage in the AlAs layer, which explains why the Al(2*p*) signal scarcely moves upon cooling in the case of the Si-containing heterostructure (Fig. 8). To the contrary, the RT band profiles proposed for the GaAs/AlAs(100) and GaAs/Be/AlAs(100) heterostructures indicate the existence of *upward* band bending in the AlAs region [see the solid lines in Figs. 9(a) and 9(c)]. Thus, a photovoltage can be induced, producing band flattening in the AlAs layer, and consequently a shift of the Al(2*p*) signal toward *lower* kinetic energies, as observed experimentally (Fig. 8).

The Al(2*p*) signal originates close to the front AlAs/GaAs interface. The kinetic energy expected for the Al(2*p*) signal if the bands were completely flat all along the *n*-GaAs substrate and the AlAs buried layer in any of our GaAs/AlAs/*n*-GaAs(100) samples is marked in Fig. 8 by a vertical dotted line, and corresponds to a value $E_k=15.24$ eV.[44] At LT the Al(2*p*) centroids appear at kinetic energies of 15.28, 15.09, and 15.29 eV for the GaAs/AlAs(100), GaAs/Si/AlAs(100), and GaAs/Be/AlAs(100) samples, respectively. The position of the Al(2*p*) peaks measured on the three types of heterostructures at LT is thus very close to the ''flatband'' energy. Taking into account the fact that the band profiles proposed for the AlAs layer and the *n*-GaAs substrate of the GaAs/AlAs(100) and GaAs/Be/AlAs(100) samples at RT favor the establishment of a photovoltage, it is reasonable to conclude that the bands become completely flat from the front AlAs/GaAs interface down to the deep *n*-GaAs bulk, as depicted in Fig. 9 (dotted lines). Note that the band profile proposed for the Si-containing structure is already flat at RT along this region.

The Ga(3*d*) signal and the leading edge of the valence-band spectrum mainly originate close to the GaAs surface. In a *hypothetical* situation where the bands were completely flat all along the GaAs/AlAs/*n*-GaAs(100) heterostructures, the Ga(3*d*) signal and the valence-band leading edge would appear at kinetic energies of 69.71 and 88.57 eV, respectively,[45] assuming a *constant* band-offset value upon intralayer insertion. Such flat-band energy positions are marked in Fig. 8 as vertical dotted lines. The Ga(3*d*) signals and the leading edges of the valence-band spectra for the intralayer-containing samples are seen to deviate from such flat-band positions, at both RT and LT (Fig. 8). The shifts of the Ga(3*d*) and valence-band-edge signals cannot be explained as being due to light-induced flattening of the GaAs-overlayer bands, since the constancy of the Al(2*p*)-to-Ga(3*d*) energy separation upon cooling (Fig. 8) implies that the overlayer band bending does not change. However, these shifts can be well understood as being a consequence of the light-induced flattening of the AlAs bands, which additionally causes the bands of the GaAs overlayer to be rigidly ''pulled down'' toward higher binding energies (as depicted in Fig. 9), so that the Ga(3*d*) and valence-band-edge signals are shifted toward lower kinetic energies. The persistence of the overlayer band bending is probably due to the role played by the interface band discontinuities, which act as energy barriers preventing the transport of the photogenerated carriers through the interface. In the three heterostructures considered, the band discontinuities existing at the front AlAs–GaAs interface restrict the spatial separation of the electron-hole pairs photogenerated within the overlayer to the thickness of the overlayer itself, which is only 2 nm. The

overlap of the electron and hole wave functions inside the thin overlayer is considerable (the Bohr's radius of free electrons is ~10 nm and of free holes ~3 nm). Therefore, the electron-hole recombination is high, and the establishment of a photovoltage in the overlayer region is ineffective.

IV. CONCLUSIONS

We have demonstrated, through the examination of polar and nonpolar interfaces, intralayers of different doping type, and photoelectron spectra recorded under conditions where a surface photovoltage exists, that no change in the band offset of the heterojunction upon intralayer insertion needs to be invoked in order to arrive at a consistent description of our results. Indeed, some of our results are in direct contradiction of the interface-capacitor model previously invoked to explain such type of photoemission data. Rather, we propose an overlayer-capacitor model in which charge separation between the surface and the intralayer builds up a strong electric field in the overlayer. Hence, the photoemission results are explained in terms of band-bending profile changes.

ACKNOWLEDGMENTS

The authors gratefully acknowledge P. Schützendübe and H. P. Schönherr for their expert MBE assistance, W. Braun for the flexibility in the beam-time scheduling, necessary to coordinate the synchrotron experiments performed at BESSY with the MBE sample growth, J. A. Martín-Gago, C. Rojas, F. Schneider, C. Polop, S.-A. Ding, and S. Barman for technical assistance during the synchrotron beam times, and H. Kostial, H. Yang, and A. Yamada for valuable discussions. One of the authors (M. M.) acknowledges financial aid from the Comunidad Autónoma de Madrid (Spain). This work was partially supported by the Spanish Dirección General de Investigación Científica y Técnica under Grant Nos. PB98-524 and PB97-1195. The work at BESSY was supported by the EU Human Capital and Mobility Programme under Contract No. CHGE-CT93-0027.

[1]C. G. Van de Walle and R. M. Martin, Phys. Rev. B **34**, 5621 (1986).
[2]C. G. Van de Walle and R. M. Martin, Phys. Rev. B **37**, 4801 (1988).
[3]S. Baroni, R. Resta, A. Baldereschi, and M. Peressi, in *Spectroscopy of Semiconductor Microstructures,* edited by G. Fasol, A. Fasolino and P. Lugli (Plenum, London, 1989), Vol. 206, p. 251.
[4]W. R. L. Lambrecht and B. Segall, Phys. Rev. B **41**, 8353 (1990).
[5]A. Baldereschi, R. Resta, M. Peressi, S. Baroni, and K. Mäder, in *Semiconductor Interfaces at the Sub-Nanometer Scale,* edited by H. W. M. Salemink and M. D. Pashley (Kluwer, Dordrecht, 1993), Vol. 243, p. 59.
[6]S. Baroni, R. Resta, and A. Baldereschi, in *Proceedings of the 19th International Conference on the Physics of Semiconductors,* edited by W. Zawadzki (Institute of Physics, Polish Academy of Sciences, Wroclaw, 1988), p. 525.
[7]A. Muñoz, N. Chetty, and R. M. Martin, Phys. Rev. B **41**, 2976 (1990).
[8]M. Peressi, S. Baroni, R. Resta, and A. Baldereschi, Phys. Rev. B **43**, 7347 (1991).
[9]D. M. Bylander and L. Kleinman, Phys. Rev. B **41**, 3509 (1990).
[10]W. A. Harrison, E. A. Kraut, J. R. Waldrop, and R. W. Grant, Phys. Rev. B **18**, 4402 (1978).
[11]A. Franciosi and C. G. Van de Walle, Surf. Sci. Rep. **25**, 1 (1996).
[12]R. M. Martin, J. Vac. Sci. Technol. **17**, 978 (1980).
[13]R. G. Dandrea, S. Froyen, and A. Zunger, Phys. Rev. B **42**, 3213 (1990).
[14]G. Biasiol, L. Sorba, G. Bratina, R. Nicolini, A. Franciosi, M. Peressi, S. Baroni, R. Resta, and A. Baldereschi, Phys. Rev. Lett. **69**, 1283 (1992).
[15]E. A. Kraut, R. W. Grant, J. R. Waldrop, and S. P. Kowalczyk, Phys. Rev. Lett. **44**, 1620 (1980).
[16]R. W. Grant, E. A. Kraut, S. P. Kowalczyk, and J. R. Waldrop, J. Vac. Sci. Technol. B **1**, 320 (1983).
[17]E. A. Kraut, R. W. Grant, J. R. Waldrop, and S. P. Kowalczyk, Phys. Rev. B **28**, 1965 (1983).
[18]L. Sorba, G. Bratina, G. Ceccone, A. Antonini, J. F. Walker, M. Micovic, and A. Franciosi, Phys. Rev. B **43**, 2450 (1991).
[19]M. Akazawa, H. Hasegawa, H. Tomozawa, and H. Fujikura, Jpn. J. Appl. Phys., Part 2 **31**, L1012 (1992).
[20]Y. Hashimoto, G. Tanaka, and T. Ikoma, J. Vac. Sci. Technol. B **12**, 125 (1994).
[21]M. Moreno, H. Yang, M. Höricke, M. Alonso, J. A. Martín-Gago, R. Hey, K. Horn, J. L. Sacedón, and K. H. Ploog, Phys. Rev. B **57**, 12314 (1998).
[22]M. Moreno, J. L. Sacedón, M. Alonso, M. Höricke, R. Hey, J. Avila, M. C. Asensio, K. Horn, and K. H. Ploog, Phys. Rev. B **58**, 13767 (1998).
[23]T. Ogama, J. Appl. Phys. **64**, 753 (1988).
[24]G. Margaritondo, F. Gozzo, and C. Coluzza, Phys. Rev. B **47**, 9907 (1993).
[25]M. Alonso, R. Cimino, and K. Horn, Phys. Rev. Lett. **64**, 1947 (1990).
[26]M. Alonso, R. Cimino, C. Maierhofer, T. Chassé, W. Braun, and K. Horn, J. Vac. Sci. Technol. B **8**, 955 (1990).
[27]S. Chang, I. M. Vitomirov, L. J. Brillson, D. F. Rioux, P. D. Kirchner, G. D. Pettit, J. M. Woodall, and M. H. Hecht, Phys. Rev. B **41**, 12299 (1990).
[28]D. Mao, A. Kahn, M. Marsi, and G. Margaritondo, Phys. Rev. B **42**, 3228 (1990).
[29]M. Alonso, R. Cimino, and K. Horn, J. Vac. Sci. Technol. A **9**, 891 (1991).
[30]T. U. Kampen, D. Troost, X. Y. Hou, L. Koenders, and W. Mönch, J. Vac. Sci. Technol. B **9**, 2095 (1991).
[31]A. Bauer, M. Prietsch, S. Molodtsov, C. Laubschat, and G. Kaindl, J. Vac. Sci. Technol. B **9**, 2108 (1991).
[32]D. A. Evans, T. P. Chen, T. Chassé, and K. Horn, Appl. Surf. Sci. **56–58**, 233 (1992).
[33]R. Cimino, A. Gearante, M. Alonso, and K. Horn, Appl. Surf. Sci. **56–58**, 151 (1992).
[34]K. Horn, M. Alonso, and R. Cimino, Appl. Surf. Sci. **56–58**, 271 (1992).
[35]D. Mao, M. Santos, M. Shayegan, A. Kahn, G. Le Lay, Y. Hwu, G. Margaritondo, L. T. Florez, and J. P. Harbison, Phys. Rev. B **45**, 1273 (1992).
[36]M. H. Hecht, Phys. Rev. B **41**, 7918 (1990).
[37]M. H. Hecht, J. Vac. Sci. Technol. B **8**, 1018 (1990).
[38]L. Däweritz, H. Kostial, R. Hey, M. Ramsteiner, J. Wagner, M. Maier, J. Behrend, and M. Höricke, J. Cryst. Growth **150**, 214 (1995).
[39]K. H. Ploog and L. Däweritz, Jpn. J. Appl. Phys., Part 1 **34**, 691 (1995).
[40]A. Muñoz and P. Rodríguez-Hernández, Phys. Rev. B **45**, 4502 (1992).
[41]R. H. Miwa and A. C. Ferraz, Phys. Rev. B **59**, 12499 (1999).
[42]J. F. Sampaio, S. L. S. Freire, and E. S. Alves, J. Appl. Phys. **81**, 530 (1997).
[43]J. M. Ballingall and C. E. C. Wood, J. Vac. Sci. Technol. B **1**, 162 (1983).
[44]This ''flat-band energy'' has been calculated assuming the values: $E_g^{\mathrm{GaAs}} = 1.43$ eV for the GaAs band gap, $\Delta E_V = 0.47$ eV for the GaAs/AlAs valence-band offset, and $E_{\mathrm{Al}(2p)} - E_V = -72.86$ eV for the Al(2*p*) binding energy. We have determined the valence-band offset value through PES measurements of the ''apparent'' offset in the GaAs/AlAs(100) heterostructure without an intralayer at RT, which give $\Delta E_V^* = 0.5$ eV. In order to obtain the ''real'' offset, the value of the overlayer band bending (0.03 eV, calculated by solving Poisson's equation) must be subtracted.
[45]The flat-band kinetic-energy value for the Ga(3*d*) level has been calculated assuming the value $E_{\mathrm{Ga}(3d)} - E_V = -18.86$ eV for the Ga(3*d*) binding energy.